

Is Chinese stalagmite $\delta^{18}O$ solely controlled by the Indian summer monsoon?

Dong Li^{1,2} · Liangcheng Tan^{1,3,4} • Yanjun Cai^{1,3,4} · Xiuyang Jiang⁵ · Le Ma¹ · Hai Cheng^{4,6} · R. Lawrence Edwards⁶ · Haiwei Zhang⁴ · Yongli Gao⁷ · Zhisheng An^{1,3,8}

Received: 18 November 2018 / Accepted: 5 February 2019 / Published online: 12 February 2019 © Springer-Verlag GmbH Germany, part of Springer Nature 2019

Abstract

As a unique continental archive, speleothem has been widely used in reconstructing paleoclimate change. However, the interpretation of Chinese speleothems $\delta^{18}O$ has remained a subject of debate. Recently, a Community Atmosphere Model version 3 (CAM3) study indicated that the stalagmite $\delta^{18}O$ from eastern China reflected the Indian summer monsoon (ISM) intensity rather than the East Asian summer monsoon (EASM) intensity during Heinrich events. Here, we present a high-resolution speleothem $\delta^{18}O$ record from Xianglong Cave in Shaanxi province, China, covering the period of 25.5–10.9 ka BP. The XL15 record shows similar variations with ice core record from Greenland and other climate records from China and India on millennial scale, including Heinrich 2 (H2), Heinrich 1 (H1), Bølling–Allerød (BA) and Younger Dryas (YD) events, supporting the connection between the Asian monsoon and northern high latitude climate. The $\delta^{18}O$ amplitude of our record is larger than or similar to the stalagmite $\delta^{18}O$ records from India during these events. In addition, differences of stalagmite $\delta^{18}O$ in eastern China and the ISM region were observed on glacial-interglacial as well as decadal timescales. That means the ISM is not the sole controlling factor of Chinese stalagmite $\delta^{18}O$ during Heinrich events. When subtracting the Indian stalagmite $\delta^{18}O$ series from our XL15 record during H1 period, we found a significant negative correlation with sea surface temperature (SST) record of Western Pacific Warm Pool (WPWP). Consequently, our study suggests that the Chinese stalagmite $\delta^{18}O$ is controlled by both the ISM and EASM on orbital-, millennial-, and decadal timescales.

Keywords Chinese stalagmite $\cdot \delta^{18}O \cdot \text{Indian summer monsoon} \cdot \text{East Asian summer monsoon} \cdot \text{Heinrich events}$

1 Introduction

Among the global climatic system, the Asian summer monsoon (ASM) is one of the most important parts as well as the most active components. About 60% of the world's population are under the influence of the ASM. Therefore, changes of monsoonal rainfall affects the livelihood and well-being

of societies directly. Spring-time solar heating of the Asian continent overturns the atmosphere circulation and initiates the ASM (Webster et al. 1998; Ding and Chan 2005; Cheng et al. 2012). With the increase in land-sea temperature contrast, the strong atmospheric circulation transports abundant moisture from distal ocean into most part of Asia (Cheng et al. 2012). That is to say, the ASM intensity is a concept of

- State Key Laboratory of Loess and Quaternary Geology, Institute of Earth Environment, Chinese Academy of Sciences, Xi'an 710061, China
- University of Chinese Academy of Sciences, Beijing 100049, China
- Center for Excellence in Quaternary Science and Global Change, Chinese Academy of Sciences, Xi'an 710061, China
- Institute of Global Environmental Change, Xi'an Jiaotong University, Xi'an 710049, China

- College of Geography Science, Fujian Normal University, Fuzhou 350007, China
- Department of Earth Sciences, University of Minnesota, Minneapolis, MN 55455, USA
- Department of Geological Sciences, Center for Water Research, University of Texas at San Antonio, San Antonio, TX 78249, USA
- Open Studio for Oceanic-Continental Climate and Environment Changes, Pilot National Laboratory for Marine Science and Technology, Qingdao 266061, China



wind field and could control the rainfall of the overall Asian monsoon region, but not necessarily the rainfall in a certain region (Cheng et al. 2009, 2016). The ASM is composed of two sub-systems: the Indian summer monsoon (ISM) and the East Asian summer monsoon (EASM), which are independent to but also interacting with each other (Wang and Lin 2002; Ding and Chan 2005). Paleoclimatologists have done many studies in the ASM region and obtained abundant paleoclimatic archives and proxies on different timescales (An et al. 2000; Wang et al. 2001, 2005, 2008; Fleitmann et al. 2003, 2007; Hong et al. 2005; Yancheva et al. 2007; Cheng et al. 2009, 2016; Xu et al. 2012; Yang et al. 2014a; Yi et al. 2018; Zhang et al. 2018). Therein, speleothems are unique continental archives due to their precise absolute chronologies, continuous or semi-continuous precipitation. multiproxies and extensive terrestrial distributions (Wong and Breecker 2015).

Over the past two decades, speleothem studies have become more and more prevalent in reconstructing climate changes over the ASM region. However, there have been some controversies concerning how to interpret speleothem δ^{18} O variations in eastern China. For example, Wang et al. (2001) suggested that changes of stalagmite δ^{18} O reflect variations in the proportion of the amount of summer to winter precipitation. Low δ^{18} O value indicates higher proportion of summer monsoon precipitation, i.e., stronger EASM intensity. Yuan et al. (2004) invoked Rayleigh fractionation theory to demonstrate that the fraction of water vapor rained out between the moisture source (tropical Indo-Pacific) and cave site could be responsible for the observed Chinese stalagmite δ^{18} O variations. Decreased δ^{18} O values resulted from the condensation of larger proportion of water vapor during transportation path (Yuan et al. 2004). Following this theory, Hu et al. (2008) reconstructed the monsoon precipitation changes in southwestern China by using the δ^{18} O differences of two coeval stalagmites from Heshang Cave in central China and Dongge Cave in southwestern China. Cheng et al. (2009, 2016) attributed variations of stalagmite δ^{18} O values to changes of the summer monsoon intensity or summer monsoon rainfall due to the low δ^{18} O value of the summer monsoon precipitation. Depleted δ^{18} O of stalagmite implies more spatially integrated monsoon precipitation between the cave site and the monsoon moisture sources, in other words, strengthened monsoon intensity (Cheng et al. 2016). This is also supported by the latest modeling results (Liu et al. 2014). All of the above viewpoints link stalagmite $\delta^{18}O$ with summer monsoon intensity and amount of rainfall in a large region on orbital to millennial scales. Cai et al. (2010) and Tan et al. (2015) suggested that ice volume, ocean circulation, and boundary conditions of the East Asian continent were relatively stable over shorter timescales, and speleothems δ^{18} O may reflect local rainfall variability in some specific areas. For example, there is a distinct inverse relationship between rainfall and speleothems δ^{18} O variations in southwestern China, where most of the moisture is from the Bay of Bengal (Tan et al. 2017).

Based on the discrepancies between stalagmite $\delta^{18}O$ from southern China and loess/palaeosol magnetic records from northern China (e.g., Maher and Hu 2006) during the Holocene, Maher (2008), Maher and Thompson (2012) and Maher (2016) argued that the Chinese speleothem δ¹⁸O records reflect not rainfall amounts but rainfall source changes, ISM-sourced vapor being far-travelled and isotopically light, and EASM-sourced vapor having more proximal source and isotopically heavy. Tan (2009, 2011, 2014) suggested that stalagmite $\delta^{18}O$ within monsoonal China is controlled by the "circulation effect" on different timescales. When the West Pacific Subtropical High (WPSH) extends southwestward, more water vapor from the western Pacific transports to eastern China and causes heavier $\delta^{18}O$ in the precipitation and stalagmites. In contrast, when the WPSH retreats northeastward, more water vapor from the Indian Ocean transports to eastern China and causes lighter δ^{18} O in the precipitation and stalagmites.

Recently, Pausata et al. (2011) suggested that Chinese stalagmite $\delta^{18}O$ was controlled by variations in the ISM intensity through a modeled Heinrich 1 (H1) event. The Indian monsoon intensity was weak during Heinrich events and water vapor exported to eastern China was isotopically enriched, which caused the positive shift of stalagmite $\delta^{18}O$ in eastern China. In addition, their simulation indicated that the amplitude of precipitation $\delta^{18}O$ signal weakened with the increased distance from the moisture source to eastern China (Pausata et al. 2011). Following the view of Pausata et al. (2011), Johnson (2011), Yang et al. (2014b) and Liu et al. (2015) also considered Chinese speleothem $\delta^{18}O$ as an indicator of rainfall changes in the ISM region rather than the EASM variability.

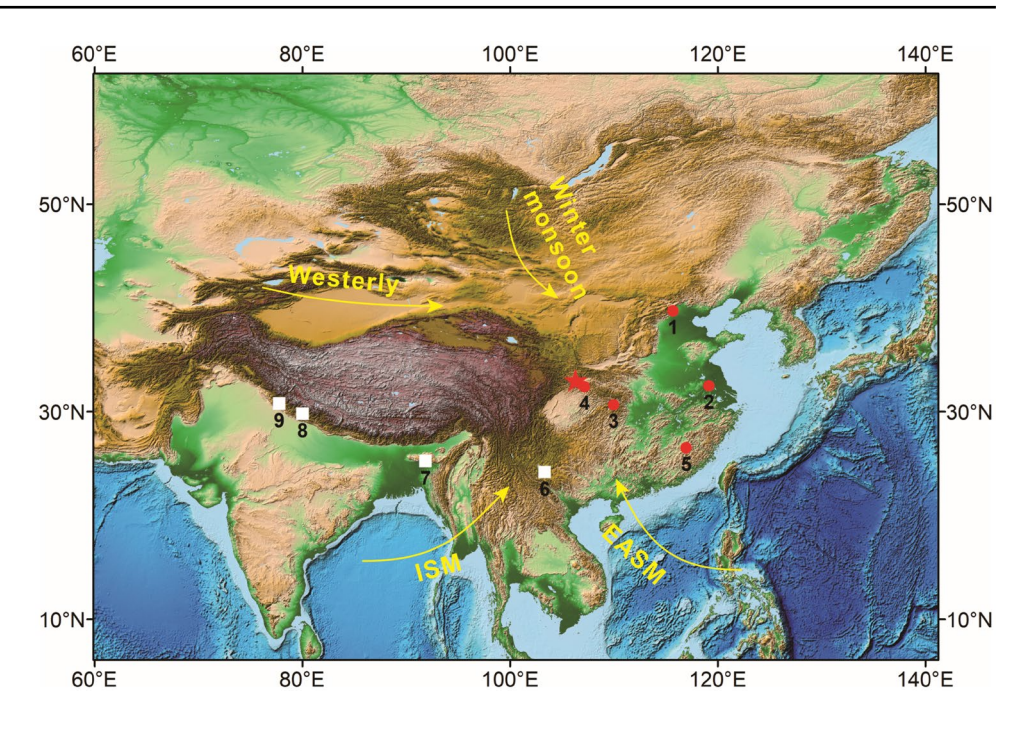
Here, we establish a new high-resolution stalagmite $\delta^{18}O$ record from Xianglong Cave in Shaanxi province, covering the period of 25.5–10.9 ka BP. We compared the XL15 record with other stalagmite $\delta^{18}O$ records from China and India. Our study, together with other evidence and records, suggests that both the ISM and EASM could influence the stalagmite $\delta^{18}O$ signal in eastern China on orbital-, millennial-, and decadal timescales.

2 Cave site and sample

Xianglong Cave [32°59′51″N, 106°19′41″E, 863 m asl] is located on the southern side of the Qinling Mountains, Shaanxi province (Fig. 1). This region is at the western margin of WPSH, and is strongly affected by the ASM. In summer (June–October), the northward summer monsoon brings humid/warm air and provides abundant monsoonal



Fig. 1 Location of Xianglong Cave (red five-pointed star). Numbers indicate locations of the following caves: (1) Kulishu (Ma et al. 2012; Orland et al. 2015), (2) Hulu (Wang et al. 2001), (3) Haozhu (Zhang et al. 2016), (4) Songjia (Zhou et al. 2008), (5) Xianyun (Cui et al. 2017), (6) Xiaobailong (Cai et al. 2015; Tan et al. 2017), (7) Mawmluh (Dutt et al. 2015), (8) Timta (Sinha et al. 2005), (9) Bittoo (Kathayat et al. 2016). Yellow arrows indicate directions of the East Asian summer monsoon (EASM), Indian summer monsoon (ISM), East Asian winter monsoon, and westerly



precipitation at the site (> 70%, Liu et al. 2003). In winter, the southward winter monsoon carries dry/cold air. The records of Ningqiang meteorological station, which is located about 20 km southwest of Xianglong Cave, show that the mean annual air temperature of the study area is 13 °C, and the mean annual rainfall is 1100 mm (Tan et al. 2013). Monitoring of precipitation at the cave site between June 2010 and June 2011 shows that the δ^{18} O of precipitation is lower during summer and autumn (with an average value of -8.6%) than winter and spring (with an average value of -4.4%) (Tan et al. 2015).

The bedrock of Xianglong Cave is Early Proterozoic dolomite and the known length of cave exceeds 1200 m (Tan et al. 2013). Plentiful drip water is observed inside the cave even during wintertime and the humidity of the inner cave is about 100% all year long. There are abundant secondary carbonate deposits in the cave: stalactites and stalagmites, which are in various shapes. Some stalagmites and stalactites were broken during the tourism development.

Stalagmite XL15 was collected in the inner chamber. The total length of XL15 is 40 cm with a cylindrical shape. The deposition center is relatively stable from bottom to top. The stalagmite is primarily composed of calcite with a small amount on the edge of the upper part composed of aragonite



Fig. 2 Polished section of XL15. Black bars indicate positions of U-Th dates. Black dashed line shows the drilling path for the analysis of stable isotopes

(Fig. 2). The halved and polished stalagmite section shows clear growth layers.



3 Methods

About 50–100 mg powder were drilled parallel to the growth planes of the stalagmites for U-Th dating. We obtained 17 subsamples from the bottom to top, as the drilling positions shown in Fig. 2. Measurements of Th and U isotopes were performed on a multi-collector inductively coupled plasma mass spectrometer (MC-ICPMS, Thermo-Finnigan Neptune). The procedure for chemical separation of Th and U was described in Edwards et al. (1987), the details on instrumental methods should refer to Cheng et al. (2013).

Subsamples for O and C isotope analysis were collected along the central growth axis at an average interval of 1 mm. A total of 344 subsamples were measured by Finnigan MAT-253 mass spectrometer equipped with an automated carbonate preparation system (Gasbench II). Results are reported in per mil (‰), relative to the Vienna Pee Dee Belemnite (VPDB). Precision of δ^{18} O values is better than 0.12% at the 2σ level.

4 Results

4.1 Chronology

U series dating data are listed in Table 1. Results show that the ²³⁸U and ²³²Th concentrations are 140–238 ppb and 271-8750 ppt, respectively. Uncertainties of corrected ²³⁰Th dates range from 50 to 300 years. All ²³⁰Th ages are in stratigraphic order within the range of errors. We compared the age models of linear interpolation, COPRA (Breitenbach et al. 2012) and StalAge (Scholz and Hoffmann 2011), and chose the linear interpolation model to establish the chronology of XL15 (Fig. 3) due to two reasons. Firstly, both COPRA and StalAge use the Monte-Carlo simulation. However, when growth rates of stalagmite in the boundary (e.g., the top or the bottom of the stalagmite) change drastically, the Monte-Carlo simulation may not build the true growth history (Scholz and Hoffmann 2011). As for XL15, the growth rate between the first and second dates (XL15-1 and XL15-2) is 124 µm/a, while the growth rate between the second and third dates (XL15-2 and XL15-2c) is 17 µm/a (Fig. 2). Due to the distinctive changes of growth rate, both COPRA and StalAge age models consider the first age datum as an outlier (Fig. 3) and exclude it in the chronology. Secondly, the linear interpolation was widely used to build age models in previous studies. In order to compare with previous studies, we chose the linear interpolation method. Results show that XL15 was continuously deposited from 25.5 to 10.9 ka BP.



4.2 The δ^{18} O record

The $\delta^{18}O$ record of XL15 is shown in Fig. 4b. The $\delta^{18}O$ of XL15 fluctuated between -8.27% and -2.74%, with a mean temporal resolution of ~37 years. From 25.5 to 24.5 ka BP, the $\delta^{18}O$ fluctuated around -5.6%. Afterwards, the $\delta^{18}O$ values increased significantly during 24.5 and 23.7 ka BP. Then, the $\delta^{18}O$ decreased and fluctuated around -5.3%. From 17.9 ka BP, the $\delta^{18}O$ values decreased rapidly to -8.01%, followed by a dramatic increase to -2.74% at 16.1 ka BP, which is the heaviest value of the entire $\delta^{18}O$ record. After this period, the $\delta^{18}O$ decreased and increased again to -5.15% at 11.8 ka BP.

4.3 Test of equilibrium deposition

An essential prerequisite for using stalagmite δ^{18} O to reconstruct paleoclimate change is that the stalagmite was precipitated under isotopic equilibrium conditions. Two commonly used equilibrium tests are Hendy Test (Hendy 1971) and Replication Test (Dorale and Liu 2009). The main contents of Hendy Test include: (1) δ^{18} O values of the same growth layer remain stable without enrichment trend to the edge; (2) there is no significantly positive correlation between δ^{13} C and δ^{18} O in the same growth layer. In recent years, however, the validity of the Hendy Test is increasingly challenged (Fairchild et al. 2006; Romanov et al. 2008; Dorale and Liu 2009). It is difficult to ensure that the samples used for Hendy Test are taken from the same growth layer during the actual sampling process (Fairchild et al. 2006). In addition, some studies showed that while the edge of the stalagmite was under kinetic fractionation, its center could still be under the equilibrium fractionation (Talma and Vogel 1992; Spötl and Mangini 2002). Another widely used equilibrium test is the replication of δ^{18} O records from different stalagmites in the same cave or from different caves (Dorale et al. 1998; Wang et al. 2001; Dorale and Liu 2009; Cai et al. 2010). The $\delta^{18}O$ of XL15 and Hulu record show broad similarities (r = 0.774, p < 0.01) during overlapping growth interval considering their dating errors and resolution difference (Fig. 4). The replication of these two records indicates that kinetic fractionation has minimal effect and the δ^{18} O variations of our stalagmite were mainly of climatic origin.

5 Discussion

5.1 Interpretation of speleothem δ¹⁸O

Under isotopic equilibrium conditions, stalagmite $\delta^{18}O$ is controlled by the cave temperature (-0.23%c/°C, O'Neil et al. 1969) and the $\delta^{18}O$ of drip water (Hendy 1971). Recently, Caley et al. (2014) suggested that regions within

Table 1 230 Th dating results of XL15. The error is 2σ error

date in dating togatic of the circle is 20 circle	me ream																		
Sample number Depth	Depth	238U		²³² Th		230Th/232Th	Th	8 ²³⁴ U*		²³⁰ Th/ ²³⁸ U	5	Age (year)	- T	Age (year)		8 ²³⁴ U _{Initial} **	l	Age (year	
	шш	(qdd)		(bbt)		(atomic	$(atomic \times 10^{-9})$	(measured)	(pa	(activity)		(uncorrected)	(ted)	(corrected)	1)	(corrected)	_	BP)*** (corrected)	(1
XL15-1	6	144.9	±0.3	1615	±32	224	+5	536.1	±4.8	0.1514	± 0.0008	11,246	±72	11,037	±164	553	+5	10,976	±164
XL15-2	78.5	191.0	±0.5	469	6+	1055	± 22	541.6	±5.4	0.1570	± 0.0006	11,644	99 =	11,598	±73	260	9∓	11,537	±73
XL15-2c	99.5	204.9	± 0.2	648	±13	904	+ 18	542.8	± 1.5	0.1733	± 0.0004	12,903	±33	12,844	±53	563	+ 2	12,778	±53
XL15-1a	113.5	185.9	± 0.3	1778	+ 36	323	±7	538.4	± 2.3	0.1875	± 0.0009	14,067	±75	13,888	±147	260	+ 2	13,826	± 147
XL15-2a	134.5	197.3	± 0.3	44	6+	1362	± 28	511.2	±2.7	0.1848	± 0.0007	14,123	99 =	14,080	±72	532	+3	14,018	±72
XL15-3	159	220.6	±0.4	716	±20	747	± 15	515.0	± 3.4	0.2005	± 0.0006	15,361	± 63	15,277	98∓	538	+ 14	15,216	98∓
XL15-3a	185.5	238.0	± 0.3	2997	709∓	283	9#	525.7	± 2.4	0.2163	± 0.0008	16,531	±72	16,294	± 182	550	+3	16,232	± 182
XL15-4	229	167.3	± 0.3	6230	± 125	105	±2	531.7	±3.5	0.2366	±0.0010	18,119	± 94	17,422	± 502	559	+ 1	17,361	± 502
XL15-2b	236	173.7	±0.4	4129	±83	164	+3	510.7	±3.3	0.2363	±0.0018	18,379	± 153	17,928	±353	537	+3	17,862	± 353
XL15-5a	278.5	177.6	+1.1	291	± 47	2497	±404	548.4	± 2.3	0.2479	± 0.0019	18,837	± 161	18,807	± 162	578	+ 2		± 162
XL15-6c	285.5	153.4	± 0.2	6591	± 132	103	+ 2	514.7	± 1.9	0.2694	± 0.0005	21,125	±51	20,314	±577	545	+ 2	20,248	± 577
XL15-3b	299	168.9	± 0.5	4661	± 94	164	+3	505.5	±5.0	0.2739	± 0.0019	21,651	± 184	21,127	±413	537	+5	21,061	± 413
XL15-6a	325.5	150.8	± 1.2	271	± 48	2582	±453	538.8	±2.6	0.2813	± 0.0025	21,757	± 212	21,724	± 213	573	+3	21,662	± 213
XL15-7a	354.5	183.6	± 0.2	272	±45	3293	±544	571.1	± 2.3	0.2957	± 0.0034	22,458	± 282	22,431	± 283	809	+3	22,369	± 283
XL15-7c	365	190.7	±0.4	8750	± 176	114	+ 2	535.9	± 3.1	0.3169	± 0.0008	24,863	±92	24,011	609∓	573	+3	23,945	€09
XL15-5	374	139.5	± 0.3	8226		88	+ 2	483.8	± 4.4	0.3147	± 0.0014	25,658	± 153	24,523	± 817	518	+5	24,462	± 817
XL15-6b	389	158.1	± 0.4	8998	± 175	76	+ 2	492.7	± 4.8	0.3225	± 0.0024	26,190	±238	25,142	± 778	529	+5	25,076	± 778

 $*\delta^{234}$ U = $([^{234}$ U/ 238 U $]_{activity}$ – 1)×1000

** 8^{234} U_{inital} was calculated based on ²³⁰Th age (T), i.e., 8^{234} U_{inital} = 8^{234} U_{measured} × 8^{234} V. Corrected ²³⁰Th ages assume the initial ²³⁰Th/²³²Th atomic ratio of $4.4 \pm 2.2 \times 10^{-6}$. Those are the value for a material at secular equilibrium, with the bulk earth ²³⁷Th/²³⁸U value of 3.8. The errors are arbitrarily assumed to be 50%

***B.P. stands for "Before Present" where the "Present" is defined as the year 1950 A.D



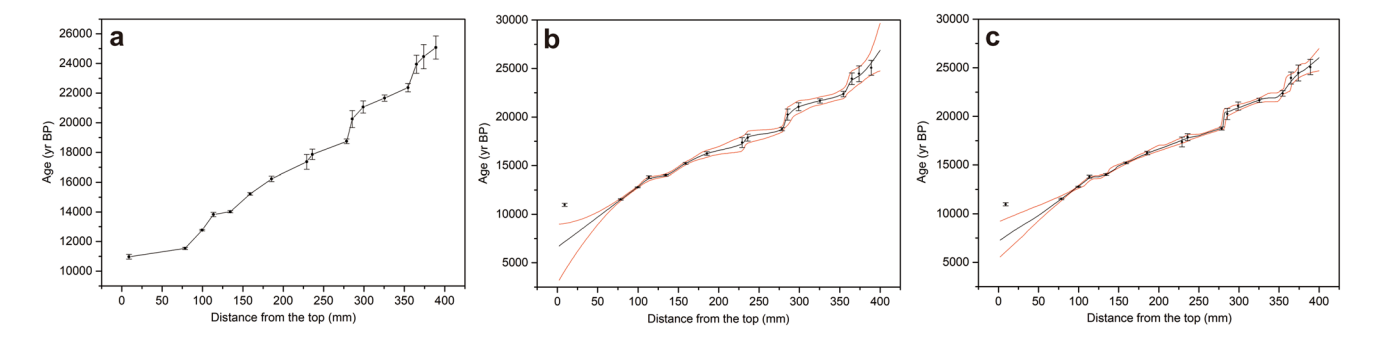


Fig. 3 Age-depth model of XL15. All ages are reported as thousand years before present (1950 AD), ka BP. The age errors indicated in the plots are 2σ error. The red lines in **b** and **c** indicate the confidence

level of 95%. a Linear interpolation method. b COPRA (Breitenbach et al. 2012). c StalAge (Scholz and Hoffmann 2011)

87°E–116°E and 17°N–33°N underwent temperature amplitude of only 3 °C over the past 150,000 years. Due to the thick roof of Xianglong Cave (~100 m, Tan et al. 2014a), the cave temperature is close to the average annual surface temperature outside the cave. A drop of 3 °C can only induce maximum amplitude of 0.7‰ in stalagmite δ^{18} O values. In addition, the temperature effect on precipitation δ^{18} O (≤0.24‰/°C) could offset the negative temperature effect on calcite-mother water fractionation in central China (Johnson et al. 2006; Cai et al. 2010; Zhou et al. 2014). Therefore, δ^{18} O variations in XL15, with the largest amplitude of ~5.53‰, were mainly controlled by the δ^{18} O of drip water, and reflected the annual weighted mean δ^{18} O of meteoric precipitation in this region (Yonge et al. 1985).

The significances of stalagmite $\delta^{18}O$ are different on different spatial-temporal scales. On orbital to millennial timescales, there are remarkably similar trends of stalagmite δ^{18} O from different caves in eastern China, suggesting that Chinese stalagmite δ^{18} O could represent changes in the overall Asian monsoon intensity or a first order change in spatially-integrated rainfall between cave site and moisture sources (Cheng et al. 2009, 2016). However, on centennial to decadal timescales, there are notably regional differences of stalagmite $\delta^{18}\text{O}$ records from northern China to southern China (Tan et al. 2009; Ma et al. 2015), indicating factors such as moisture source, i.e., "circulation effect" (Maher and Thompson 2012; Tan 2014), regional and local rainfall amount (Tan et al. 2009, 2015, 2018), and cave environment (Cosford et al. 2008) may influence the stalagmite δ^{18} O on shorter timescales.

Considering the significant positive correlation between XL15 record and Hulu record (r=0.774, p<0.01), we follow previous suggestions (Maher 2008, 2016; Cheng et al. 2009, 2016; Maher and Thompson 2012; Tan et al. 2018) in this study. The δ^{18} O of XL15 is used as an indicator of monsoon intensity on orbital and millennial timescales. Lower δ^{18} O values indicate strong summer monsoon intensity with relatively more moisture from Indian Ocean. In

contrast, higher δ^{18} O values represent weak summer monsoon intensity with relatively more moisture from western Pacific (Maher 2008, 2016; Maher and Thompson 2012; Tan 2014). Since northern China is located near the edge of the ASM, the rainfall in northern China is sensitive to the ASM intensity and hence reflected by the speleothem δ^{18} O (Zhang et al. 2008; Ma et al. 2012; Tan et al. 2014b; Orland et al. 2015; Li et al. 2017a). The good consistency between XL15 δ^{18} O record and summer precipitation reconstruction from loess sequence in the western Chinese Loess Plateau (r=-0.695, p<0.01) (Rao et al. 2013) supports this conclusion. On centennial to decadal timescales, stalagmite δ^{18} O of Xianglong Cave could reflect local monsoon rainfall as revealed by the good consistency with instrumental and historical rainfall records (Tan et al. 2015, 2018).

5.2 Millennial-scale abrupt weak monsoon events during 25.5–10.9 ka BP

During the last glacial period, global climate was punctuated by rapid millennial-scale climate fluctuations, known as Dansgaard-Oeschger events and Heinrich events (Dansgaard et al. 1984, 1993; Heinrich 1988; Bond et al. 1993). Heinrich events, as well as Younger Dryas (YD) event (also called H0 event), are thought to be triggered by the slowdown of the Atlantic meridional overturning circulation (AMOC), which were due to the collapse of the Laurentide Ice Sheet and/or Fennoscandian Ice Sheet (Bard et al. 2000; Hemming 2004; McManus et al. 2004; Marchitto et al. 2007; Muschitiello et al. 2015). Although Heinrich events were first recognized in the North Atlantic region, they are a global phenomenon (Clement and Peterson 2008; Arienzo et al. 2015). During Heinrich events, western Atlantic got colder (Arienzo et al. 2015), Europe became drier and/or colder (Genty et al. 2003, 2006), northern South America (Peterson et al. 2000) and Africa were also drier (DeMenocal et al. 2000; Gasse 2000; Stager et al. 2011). On the contrary, both southern South America (Kanner et al. 2012) and southwestern North



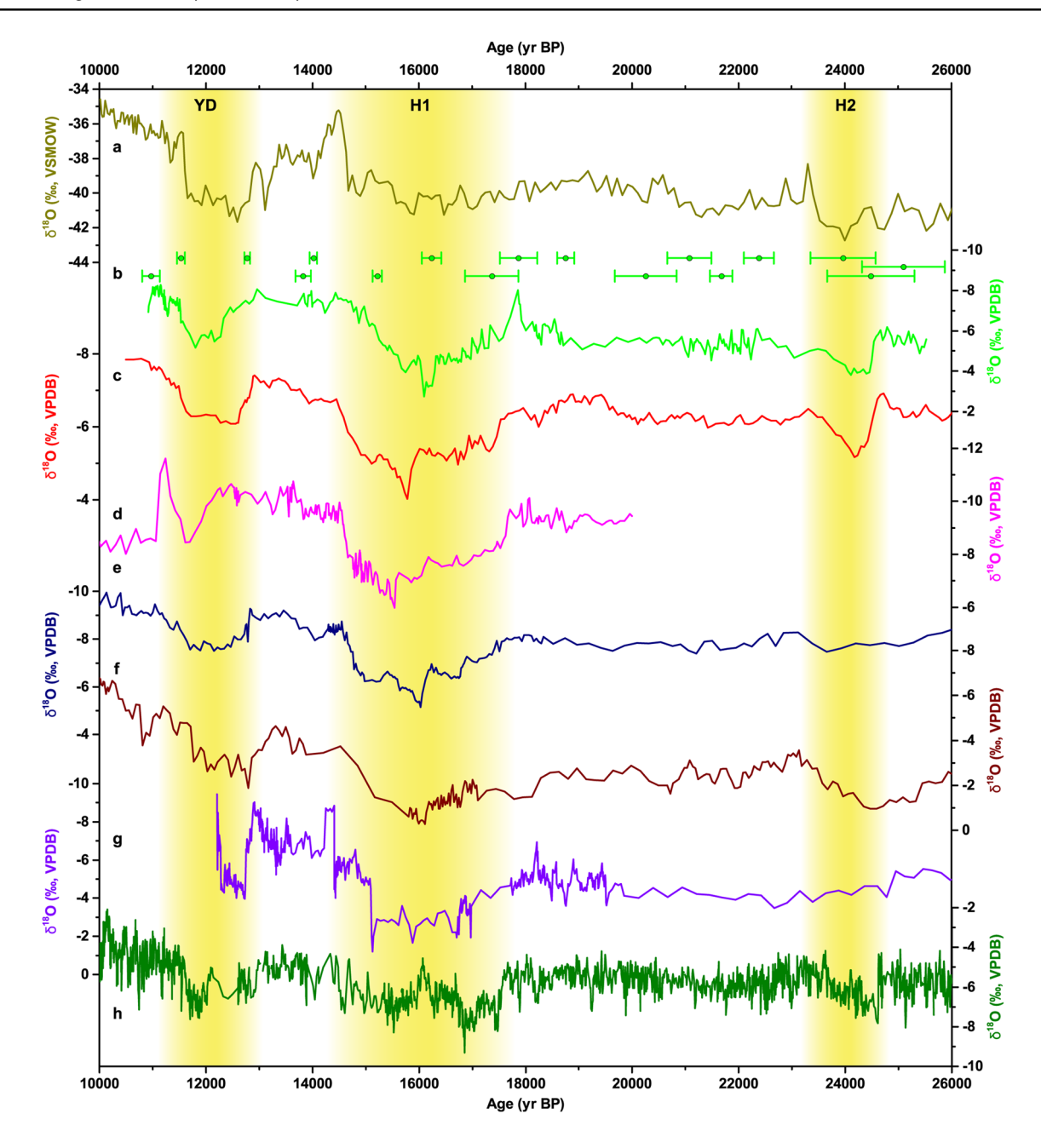


Fig. 4 Comparison of XL15 $\delta^{18}O$ series with other records. **a** The $\delta^{18}O$ record of GISP2 (Grootes and Stuiver 1997). **b** XL15 $\delta^{18}O$ record. The age error bars (2σ) are color-coded by stalagmites. **c** The $\delta^{18}O$ record from Hulu Cave (Wang et al. 2001). **d** The $\delta^{18}O$ record of Songjia Cave (Zhou et al. 2008). **e** The $\delta^{18}O$ record of Haozhu Cave

(Zhang et al. 2016). **f** The δ^{18} O record of Mawmluh Cave (Dutt et al. 2015). **g** The δ^{18} O record of Bittoo Cave (Kathayat et al. 2016). **h** The δ^{18} O record of Jaraguá Cave (Novello et al. 2017). The vertical yellow bars denote H2, H1, and YD events, respectively

America (Asmerom et al. 2010; McGee et al. 2012) became wetter, and Antarctica got warmer (Wolff et al. 2010).

The XL15 record shows similar variations with the GISP2 δ^{18} O record from northern high latitude (Fig. 4a, Grootes and Stuiver 1997), which indicates notable weak ASM during Heinrich 2 (H2), H1 and YD events, which are centered at 24.2, 16.1 and 11.8 ka BP. In contrast, strong monsoons were observed during Bølling–Allerød (BA) period, which

lasted from 14.4 to 12.8 ka BP. These results are coherent with previous conclusion that the ASM declined during Heinrich events (Wang et al. 2001). Indeed, broad similarities of XL15 record with Hulu (Wang et al. 2001), Songjia (Zhou et al. 2008), Haozhu (Zhang et al. 2016), Mawmluh (Dutt et al. 2015) and Bittoo records (Kathayat et al. 2016) indicate a clear first-order covariations of climate over the whole Asian monsoon region on millennial timescale



(Fig. 4). We also compared the XL15 record with record of Jaraguá Cave from Brazil (Novello et al. 2017). Results support the viewpoint that millennial scale events first recognized in northern high latitude regions are hemispheric (Broecker 1994), though there is an inter-hemispheric antiphase of monsoonal rainfall on both millennial and orbital timescales (Wang et al. 2007; Cheng et al. 2012; Kanner et al. 2012).

During Heinrich events, the reduction of the AMOC resulted from the collapse of the Laurentide Ice Sheet and/or Fennoscandian Ice Sheet(McManus et al. 2004; Muschitiello et al. 2015) cooled the northern mid- and high-latitudes, and thus led to the enhancement of the interhemispheric temperature contrast, pushed the Intertropical Convergence Zone (ITCZ) southward (Chiang et al. 2003; Chiang and Bitz 2005; Zhang and Delworth 2005; Broccoli et al. 2006), and might result in a weak ASM and intensified South American monsoon. Nevertheless, several studies suggested a low-latitude drive of high-latitude climate variability in Northern Hemisphere (Cane and Clement 1999; Caley et al. 2013; Kleppin et al. 2015). Thus it remains an open question.

5.3 Is Chinese stalagmite δ^{18} O solely controlled by the ISM?

Recently, a Community Atmosphere Model version 3 (CAM3) result suggested that an abrupt increase of the seaice extent in North Atlantic during H1 and YD events could decrease the temperature of the northern Indian Ocean and reduce the monsoonal precipitation over the northern Indian Ocean and Indian subcontinent (Pausata et al. 2011). Thus, the δ^{18} O of precipitation over northern India was heavier, and the water vapor moved to China through recycling was isotopically enriched. In addition, the simulation results indicated that the amplitude of precipitation δ^{18} O signal weakened with increasing distance from the moisture source (the Indian Ocean) to eastern China.

Here we compare the amplitudes of stalagmite δ^{18} O of our XL15 record and other stalagmites from eastern China with those from India during Heinrich events (Fig. 5). We calculated the amplitude of stalagmite δ^{18} O during Heinrich events by subtracting the lightest values from the heaviest. We believe this method is better than the average calculation for the following reasons: (1) the distribution of age-controlling points and dating errors may bring uncertainties to the determination of time periods of Heinrich events and Last Glacial Maximum (LGM), which further affect the average δ^{18} O values of these periods. For example, the duration of YD in Bittoo record was much shorter than that in XL15, which could be caused by dating errors (Fig. 5); (2) the heterogeneous δ^{18} O resolution within a given site (or stalagmite or record) could also affect calculated average values during Heinrich events and LGM. For example, if there are more

depleted δ^{18} O samples during some intervals, it will reduce the average values of LGM or Heinrich events. As shown in Fig. 5, the amplitude of δ^{18} O values of XL15 (~5.3‰) is similar to that from Bittoo Cave (~5.3‰, Kathayat et al. 2016) in northern India and greater than those from Mawmluh Cave (~3‰, Dutt et al. 2015) in northeastern India, Hulu (~2.9‰, Wang et al. 2001) and Songjia (~4‰, Zhou et al. 2008) records in eastern China during H1 event. In addition, the amplitude of our XL15 record is also slightly larger than that in Mawmluh record during YD and H2 events. It also shows similar amplitude (~3‰) with Timta record from northern India (Sinha et al. 2005) during YD event.

However, the heterogeneous $\delta^{18}O$ resolution could also affect the peak values. When the resolution is higher, larger $\delta^{18}O$ amplitude may be revealed. This means the peak $\delta^{18}O$ might be lighter during LGM and heavier during H1 with increased sampling resolution. However, the resolution of Bittoo record around the peak during LGM is 11 years, which is much higher than that of XL15 record (51 years). In contrast, the resolution of Bittoo record (67 years) is similar to XL15 record (40 years) around the peak during H1 event. This implies the $\delta^{18}O$ amplitude of XL15 record might be larger than Bittoo record during H1 event, if the sampling resolution was similar.

In addition to peak-to-peak calculation for $\delta^{18}O$ amplitude, we also calculated average $\delta^{18}O$ values in order to better compare our results to the modeling study of Pausata et al. (2011). We averaged the $\delta^{18}O$ values during 11.6–12.5 ka for YD, 13–14.5 ka for BA, 15.5–16.5 ka for H1 and 20–22 ka for LGM. Our results suggested that the amplitude of stalagmite $\delta^{18}O$ from LGM to H1 is ~1.1‰, ~1.4‰, ~1.5‰ for XL15, Bittoo and Mawmluh records, respectively, which are similar with the modelled results (Pausata et al. 2011). However, the amplitude of stalagmite $\delta^{18}O$ from BA to YD in XL15, Bittoo, Timta and Mawmluh record is ~1.6‰, ~1.3‰, ~1.5‰ and ~0.7‰, respectively. The $\delta^{18}O$ amplitude of XL15 is the largest among these records during YD event.

It was suggested that the temperature effect on $\delta^{18}O$ of precipitation in central China is $\leq 0.24\%$ /°C (Johnson et al. 2006), which could cancel or reduce the negative temperature effect on calcite-mother water fractionation ($\sim -0.23\%$ /°C, O'Neil et al. 1969). As a result, the temperature would have neglected influence on $\delta^{18}O$ of stalagmite in central China (Johnson et al. 2006). In addition, it was suggested that higher elevation could magnify the rainout effect, resulting in a larger amplitude of stalagmite $\delta^{18}O$ variation (Cai et al. 2012). The elevation of Bittoo, Timta, and Mawmluh Cave is ~ 3000 m, 1900 m and 1290 m, respectively, which are higher than the elevation of Xianglong Cave (863 m). Therefore, the actual amplitudes of $\delta^{18}O$ caused by climate change would be smaller in stalagmites from northern India if their elevation were the same as Xianglong Cave.



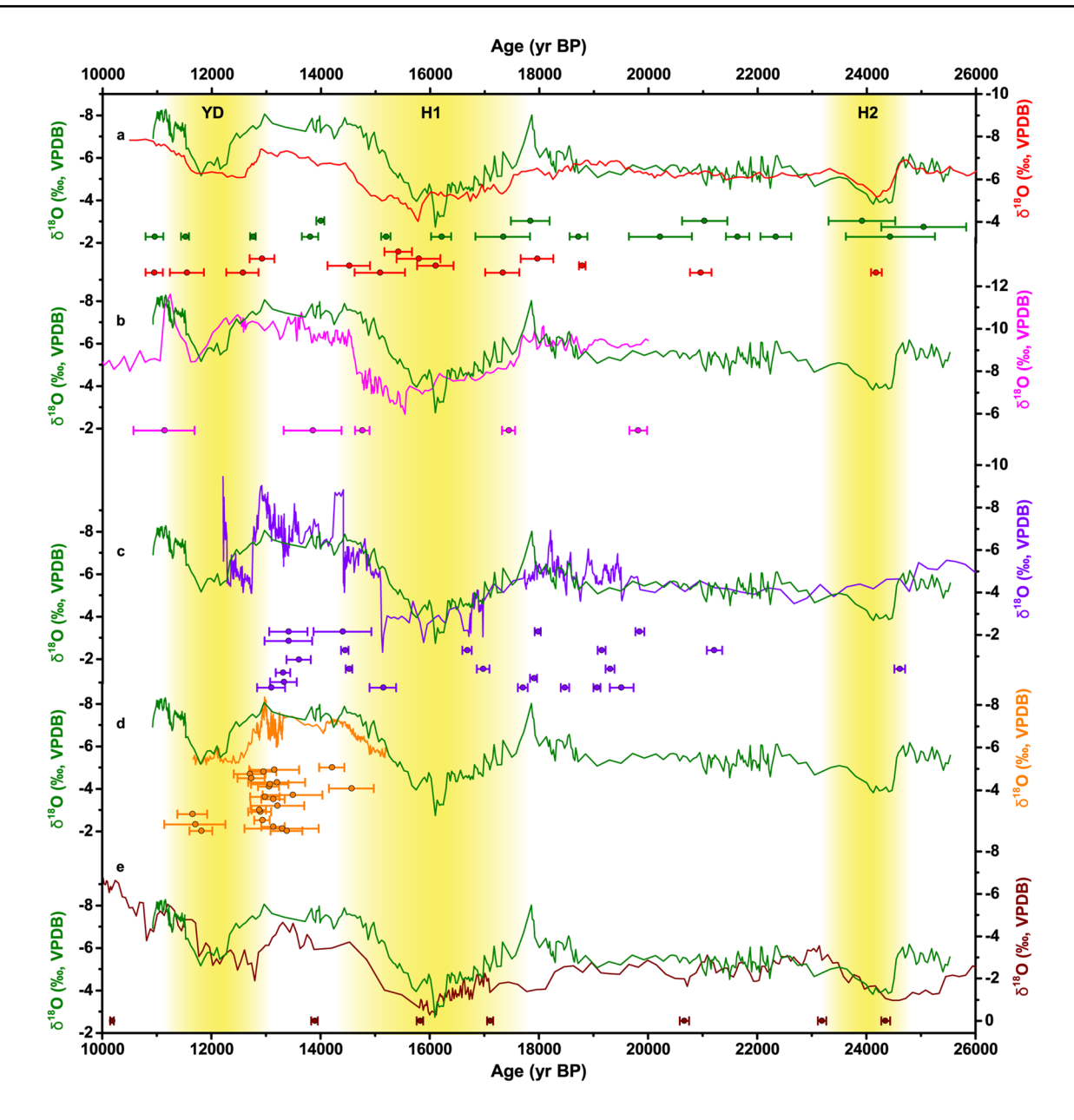


Fig. 5 The magnitude comparison of XL15 δ^{18} O record (green) and Hulu (red, Wang et al. 2001), Songjia (plum, Zhou et al. 2008), Bittoo (purple, Kathayat et al. 2016), Timta (orange, Sinha et al. 2005)

and Mawmluh (brown, Dutt et al. 2015) cave records. The age error bars (2σ) are color-coded by stalagmites. The vertical yellow bars denote H2, H1, and YD events, respectively

We indeed see the weakening $\delta^{18}O$ amplitudes from Bittoo to Timta and Mawmluh records during Heinrich events, with their decreasing elevations. This means that the amplitude of stalagmite $\delta^{18}O$ did not show a decreasing pattern from India to eastern China during Heinrich events as the model simulated (Pausata et al. 2011). Furthermore, the flux density of light $\delta^{18}O$ atoms based on observational data does not show a decreasing pattern from India to eastern China (Maher and Thompson 2012).

Moreover, a newly published stalagmite δ^{18} O record from Xianyun Cave (Cui et al. 2017), which is under the control of

typical EASM in southeast China, showed a distinct discrepancy in mutation mode of H1 event with that from Mawmluh Cave (Dutt et al. 2015). Our XL15 record, together with records from Hulu Cave (Wang et al. 2001), Songjia Cave (Zhou et al. 2008), Xianyun Cave (Cui et al. 2017) and Haozhu Cave (Zhang et al. 2016) in eastern China show three-stages (increasing-stable-increasing) in mutation mode of H1 event. In contrast, records from Bittoo Cave (Kathayat et al. 2016) and Mawmluh Cave (Dutt et al. 2015) in India show consistent increasing mode (Fig. 6). It is worth noting that the different mutation modes seen in these records might



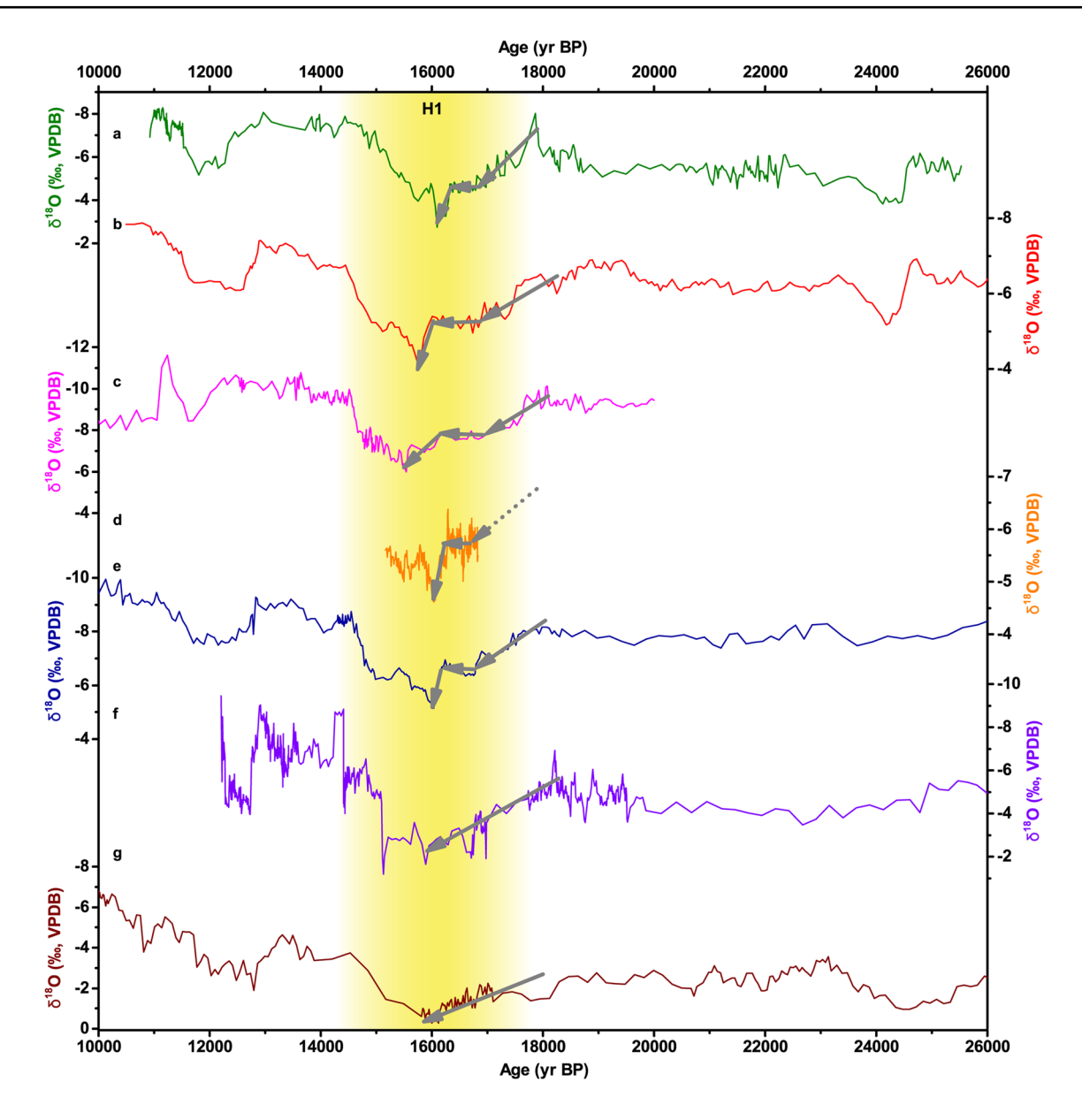


Fig. 6 Comparison of mutation mode of H1 between a XL15, b Hulu (Wang et al. 2001), c Songjia (Zhou et al. 2008), d Xianyun (Cui et al. 2017), e Haozhu (Zhang et al. 2016), f Bittoo (Kathayat et al.

2016) and ${\bf g}$ Mawmluh (Dutt et al. 2015) cave records. The vertical yellow bar denotes H1 event

be ascribed to the distribution of age-controlling points, dating errors, as well as the heterogeneity of $\delta^{18}O$ resolutions. More high-resolution and precisely dated records from both India and China are needed to verify this behavior.

Furthermore, the model of Pausata et al. (2011) did not show any changes in the seasonal distribution or annual average of precipitation at the cave sites in China associated with Heinrich events, which is in contrast with other moisture records in China (Zhou et al. 2001, 2005, 2016; Yancheva et al. 2007; Sun et al. 2010, 2011; Ma et al. 2012; Orland et al. 2015). For example, a seasonally resolved stalagmite

record from Kulishu Cave showed an increasing trend of δ^{18} O, which suggested that regional rainfall in northern China decreased during YD event (Ma et al. 2012; Orland et al. 2015). Recently, a floodplain deposition from Huai River Basin showed lower total organic carbon (TOC) and tree pollen percentage, and positive organic δ^{13} C at around 16 ka BP, which indicated a severe drought during H1 event in the Huai River Basin (Zhou et al. 2016). The decreased summer rainfall during Heinrich events was also recorded in the δ^{13} C $_{TOC}$ data of a loess profile from the western Chinese Loess Plateau (Rao et al. 2013).



Different patterns of stalagmite $\delta^{18}O$ variations from the EASM and ISM regions were also reported on other timescales. For example, a 252-kyrs-long speleothem $\delta^{18}O$ record from Xiaobailong Cave in southwestern China, which is controlled by the ISM (Cai et al. 2015), showed a significant ~100 ka cycle, which did not occur in stalagmite records from eastern China. In addition, a modern stalagmite $\delta^{18}O$ record (1912–2009 AD) from Xianglong Cave showed anti-phase variations with the stalagmite $\delta^{18}O$ record from India (Sinha et al. 2011) and the Indian monsoon rainfall index (Parthasarathy et al. 1995) during the last hundred years on decadal timescales (Tan et al. 2015). All the evidence above do not support a sole control of the ISM on Chinese stalagmite $\delta^{18}O$ variations.

5.4 Both the EASM and ISM controlled Chinese stalagmite $\delta^{18}O$

It was suggested that both the Indian Ocean and Pacific sources could influence the stalagmite δ^{18} O signal in eastern China (Maher 2008, 2016; Maher and Thompson 2012; Wang and Chen 2012; Tan 2014; Orland et al. 2015; Li et al. 2017b). The calculated change in δ^{18} O of precipitation during the YD-Holocene transition from Kulishu record is 1.3% (Orland et al. 2015), larger than the simulated result of 0.5–1.0% (Pausata et al. 2011). Orland et al. (2015) suggested that the simulated results underestimated the effect of the Pacific. Recently, based on the comparison of stalagmite δ^{18} O records between southwestern China and eastern China, along with modern precipitation δ^{18} O analysis, Li et al. (2017b) demonstrated that stalagmite δ^{18} O records and modern precipitation δ¹⁸O in Yunnan province were much more negative than the EASM regions on multiple timescales, which cannot be interpreted by the temperature, latitude, altitude, or amount effects. The only reasonable explanation is different moisture sources for the EASM and ISM regions.

Geographically, there is no clear boundary between the ISM and EASM in China. We roughly consider 100°-110°E as a broad range of boundary between the ISM and EASM (Wang and Lin 2002; Ding and Chan 2005; Li et al. 2014). In fact, the ISM and EASM are generally independent but associated with each other (Wang and Lin 2002; Ding and Chan 2005). The main components of the Indian monsoon system include: Southern Hemisphere Mascarene high, Somali cross-equatorial jet, southwest flow, Indian-Bengal low, Indian monsoon trough, and Tibetan Plateau low; while the EASM system consists of the Australian cold anticyclone, the cross-equatorial flow along the east to 100°E, southwest flow, the monsoon trough (or ITCZ) over the South China Sea and the tropical western Pacific, the WPSH, the disturbances over mid-latitudes and the Meiyu front (Tao and Chen 1985). The ISM is a tropical monsoon system but the EASM consists of both tropical and subtropical monsoon (Zhu et al. 1986; Tao and Chen 1987). Therefore, the EASM share the same component of southwest flow with the ISM, but with its own characteristics. We can divide monsoonal China into three regions: the southwest monsoon region which is affected by the Indian monsoon; the region influenced by both the EASM and ISM, as well as the region affected by the EASM (Wang and Lin 2002). Even if in the EASM region, the ISM could affect the EASM moisture and hence precipitation δ^{18} O by affecting the southwest flow. In order to extract the Pacific's signal from XL15 during H1 event, we chose Mawmluh as an ISM intensity record (Indian Ocean signal). The period of 14.5–17.5 ka BP was selected to include the duration of H1 event. We interpolated XL15 and Mawmluh δ^{18} O record with an interval of 50 years during this period, and then normalized them using the formula $x *= \frac{x_{-x_{mean}}}{x_{max} - x_{min}} (x_{mean}, x_{max}, x_{min} \text{ represent the average,}$ maximum and minimum of δ^{18} O, respectively). Finally, the normalized Mawmluh record was subtracted from the normalized XL15 record. The result can be viewed as a pure Pacific signal, i.e., subtropical monsoon (Fig. 7). When comparing the result with the sea surface temperature (SST) record from the Western Pacific Warm Pool (WPWP) (Stott et al. 2007), we found a significant negative correlation (r = -0.319, p < 0.05), with increased SST corresponding to negative δ¹⁸O values. Modern meteorological data and model simulations indicated that high SSTs in the WPWP would strengthen the upper convection around the region of Philippine, which would cause the northward shift of the WPSH and the EASM Meivu belt (Huang and Li 1987: Huang and Sun 1992; Cao et al. 2002; Huang et al. 2004), resulting in enhanced rainfall from the Pacific and negative rainfall δ^{18} O.

6 Conclusions

Based on 17 U-Th dates, we propose a high-resolution stalagmite oxygen isotope record from Xianglong Cave in Shaanxi province, covering the period of 25.5–10.9 ka BP. Our record displays a clear first-order covariations of climate with northern high latitude and other Asian monsoon records on millennial timescale. The XL15 record supports the viewpoint that millennial scale events first recognized in northern high latitude regions are hemispheric, though there is an inter-hemispheric anti-phasing of monsoonal rainfall. However, a weakened δ^{18} O signal from India to eastern China was not seen as simulated by model (Pausata et al. 2011) during Heinrich events. In addition, the differences between stalagmite records from eastern China and the ISM region were observed on glacial-interglacial scale and decadal scales. When subtracting the Indian stalagmite



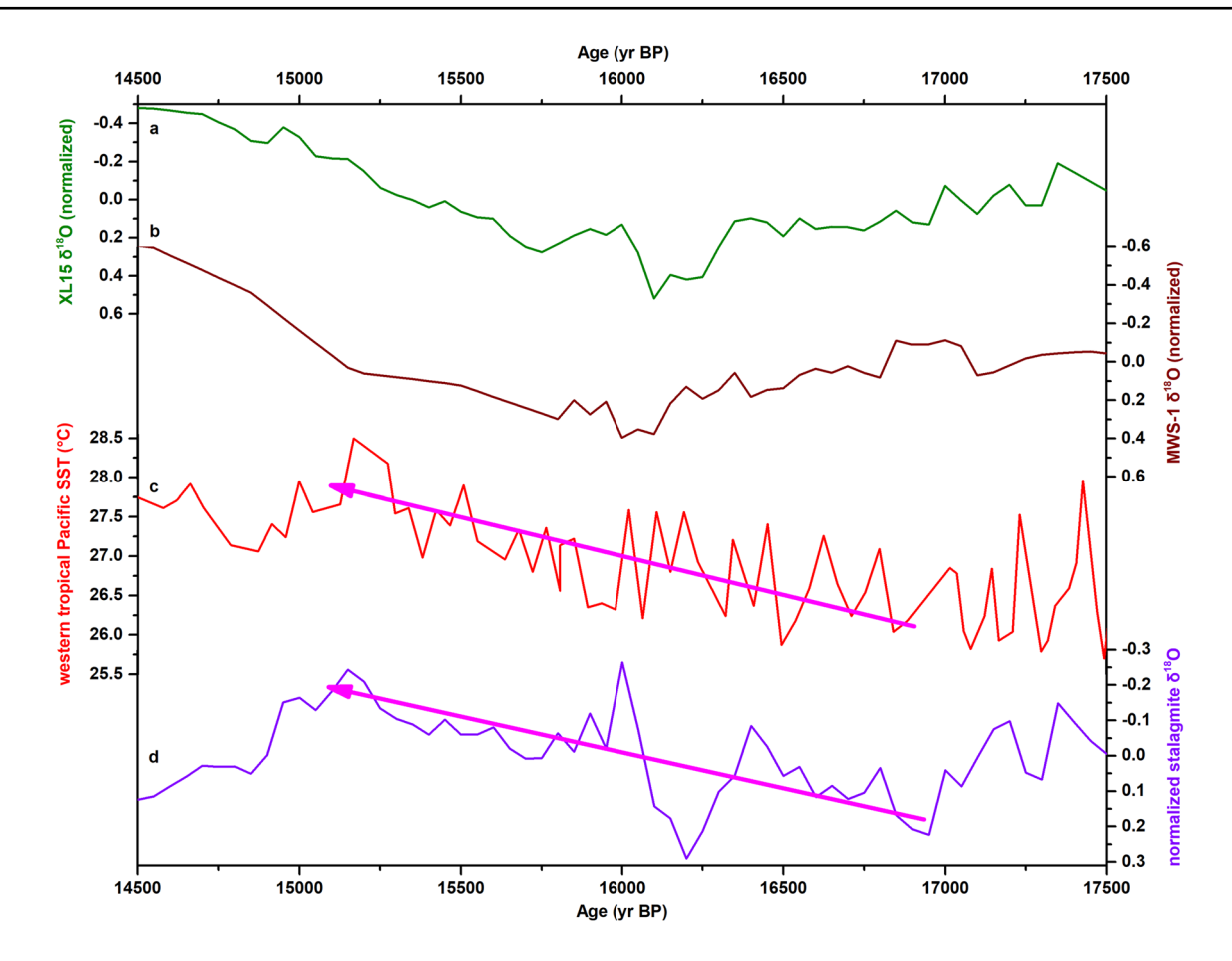


Fig. 7 Comparison of a normalized XL15 δ^{18} O record, **b** normalized Mawmluh δ^{18} O record (Dutt et al. 2015), **c** SST record from the western tropical Pacific Warm Pool (Stott et al. 2007), **d** difference between XL15 and Mawmluh record (normalized)

 $\delta^{18}O$ signal from our XL15 record during H1 period, we got the Pacific signal during H1 event for the first time. The result is significantly negatively correlated with the WPWP SST, which is consistent with modern observation and model results. Consequently, our study suggests that Chinese stalagmite $\delta^{18}O$ is controlled by both the ISM and EASM (Maher 2008, 2016; Maher and Thompson 2012; Wang and Chen 2012; Tan 2014; Orland et al. 2015; Tan et al. 2015; Li et al. 2017b).

Acknowledgements This work was supported by the National Key Research and Development Program of China (2017YFA0603401), Shaanxi Science Fund for Distinguished Young Scholars (2018JC-023), Youth Innovation Promotion Association (2012295) and West Light Foundation of Chinese Academy of Sciences. This work is a part of The "Belt & Road" Project of the Institute of Earth Environment, Chinese Academy of Sciences. We would also like to thank three anonymous reviewers for their constructive comments.

References

An ZS et al (2000) Asynchronous Holocene optimum of the East Asian monsoon. Quat Sci Rev 19:743–762

Arienzo MM et al (2015) Bahamian speleothem reveals temperature decrease associated with Heinrich stadials. Earth Planet Sci Lett 430:377–386

Asmerom Y, Polyak VJ, Burns SJ (2010) Variable winter moisture in the southwestern United States linked to rapid glacial climate shifts. Nat Geosci 3:114–117

Bard E, Rostek F, Turon JL, Gendreau S (2000) Hydrological impact of Heinrich events in the subtropical Northeast Atlantic. Science 289:1321–1324

Bond G et al (1993) Correlations between climate records from North Atlantic sediments and Greenland ice. Nature 365:143–147

Breitenbach SFM et al (2012) Constructing proxy records from age models (COPRA). Clim Past 8:1765–1779

Broccoli AJ, Dahl KA, Stouffer RJ (2006) Response of the ITCZ to northern hemisphere cooling. Geophys Res Lett 33:L01702. https://doi.org/10.1029/2005gl024546

Broecker WS (1994) Massive iceberg discharges as triggers for global climate change. Nature 372:421–424

Cai YJ et al (2010) The variation of summer monsoon precipitation in central China since the last deglaciation. Earth Planet Sci Lett 291:21–31



- Cai YJ et al (2012) The Holocene Indian monsoon variability over the southern Tibetan Plateau and its teleconnections. Earth Planet Sci Lett 335–336:135–144
- Cai YJ et al (2015) Variability of stalagmite-inferred Indian monsoon precipitation over the past 252,000 y. Proc Natl Acad Sci 112:2954–2959
- Caley T et al (2013) Southern hemisphere imprint for Indo-Asian summer monsoons during the last glacial period as revealed by Arabian Sea productivity records. Biogeosciences 10:7347–7359
- Caley T, Roche DM, Renssen H (2014) Orbital Asian summer monsoon dynamics revealed using an isotope-enabled global climate model. Nat Commun 5:5371. https://doi.org/10.1038/ ncomms6371
- Cane MA, Clement AC (1999) A role for the tropical Pacific coupled ocean-atmosphere system on Milankovitch and Millennial timescales. Part II: global impacts. In: Clark PU, Webb RS, Keigwin LD (eds) Mechanisms of global climate change at Millennial time scales. Geophysical monograph, vol 112. American Geophysical Union, Washington, pp 373–383
- Cao J, Huang RH, Xie YQ, Tao Y (2002) Research on the evolution mechanism of the western Pacific subtropical high. Sci China (Ser D) 45:659–666 (In Chinese)
- Cheng H et al (2009) Ice age terminations. Science 326:248-252
- Cheng H, Sinha A, Wang XF, Cruz FW, Edwards RL (2012) The global paleomonsoon as seen through speleothem records from Asia and the Americas. Clim Dyn 39:1045–1062
- Cheng H et al (2013) Improvements in ²³⁰Th dating, ²³⁰Th and ²³⁴U half-life values, and U-Th isotopic measurements by multi-collector inductively coupled plasma mass spectrometry. Earth Planet Sci Lett 371:82–91
- Cheng H et al (2016) The Asian monsoon over the past 640,000 years and ice age terminations. Nature 534:640–646
- Chiang JCH, Bitz CM (2005) Influence of high latitude ice cover on the marine intertropical convergence zone. Clim Dyn 25:477–496
- Chiang JCH, Biasutti M, Battisti DS (2003) Sensitivity of the Atlantic intertropical convergence zone to last glacial maximum boundary conditions. Paleoceanography 18:1094. https://doi.org/10.1029/2003PA000916
- Clement AC, Peterson LC (2008) Mechanisms of abrupt climate change of the last glacial period. Rev Geophys 46:RG4002. https://doi.org/10.1029/2006RG000204
- Cosford J et al (2008) East Asian monsoon variability since the Mid-Holocene recorded in a high-resolution, absolute-dated aragonite speleothem from eastern China. Earth Planet Sci Lett 275:296–307
- Cui MY, Xiao HY, Sun XS, Hong H, Jiang XY, Cai BG (2017) Characteristics of the Heinrich 1 abrupt climate event inferred from a speleothem record from Xianyun Cave, Fujian Province. Chin Sci Bull 62(26): 3078–3088 (In Chinese with English abstract)
- Dansgaard W et al (1984) North Atlantic climatic oscillations revealed by deep Greenland ice cores. In: Hansen JE, Takahashi T (eds) Climate processes and climate sensitivity. American Geophysical Union, Washington, pp 288–298
- Dansgaard W et al (1993) Evidence for general instability of past climate from a 250-ky ice-core record. Nature 364:218–220
- DeMenocal P et al (2000) Abrupt onset and termination of the African Humid Period: rapid climate responses to gradual insolation forcing. Quat Sci Rev 19:347–361
- Ding YH, Chan JCL (2005) The East Asian summer monsoon: an overview. Meteorol Atmos Phys 89:117–142
- Dorale JA, Liu ZH (2009) Limitations of Hendy test criteria in judging the paleoclimatic suitability of speleothems and the need for replication. J Cave Karst Stud Natl Speleol Soc Bull 71:73–80

- Dorale JA, Edwards RL, Ito E, González LA (1998) Climate and vegetation history of the midcontinent from 75 to 25 ka: a speleothem record from Crevice Cave, Missouri, USA. Science 282:1871–1874
- Dutt S et al (2015) Abrupt changes in Indian summer monsoon strength during 33,800 to 5500 years B.P. Geophys Res Lett 42:5526-5532
- Edwards RL, Chen JH, Wasserburg GJ (1987) ²³⁸U–²³⁴U–²³⁰Th–²³²Th systematic and the precise measurement of time over the past 500,000 years. Earth Planet Sci Lett 81:175–192
- Fairchild IJ et al (2006) Modification and preservation of environmental signals in speleothems. Earth Sci Rev 75:105–153
- Fleitmann D et al (2003) Holocene forcing of the Indian monsoon recorded in a stalagmite from Southern Oman. Science 300:1737–1739
- Fleitmann D et al (2007) Holocene ITCZ and Indian monsoon dynamics recorded in stalagmites from Oman and Yemen (Socotra). Quat Sci Rev 26:170–188
- Gasse F (2000) Hydrological changes in the African tropics since the Last Glacial Maximum. Quat Sci Rev 19:189–211
- Genty D et al (2003) Precise dating of Dansgaard–Oeschger climate oscillations in western Europe from stalagmite data. Nature 421(6925):833–837
- Genty D et al (2006) Timing and dynamics of the last deglaciation from European and North African δ¹³C stalagmite profiles-comparison with Chinese and south hemisphere stalagmites. Quat Sci Rev 25:2118–2142
- Grootes PM, Stuiver M (1997) Oxygen 18/16 variability in Greenland snow and ice with 10⁻³- to 10⁵-year time resolution. J Geophys Res 102:26455–26470
- Heinrich H (1988) Origin and consequences of cyclic ice rafting in the Northeast Atlantic Ocean during the past 130,000 years. Quat Res 29:142–152
- Hemming SR (2004) Heinrich events: massive late Pleistocene detritus layers of the North Atlantic and their global climate imprint. Rev Geophys 42(1):235–273
- Hendy CH (1971) The isotopic geochemistry of speleothems: I. The calculation of the effects of different modes of formation on the isotopic composition of speleothems and their applicability as palaeoclimatic indicators. Geochim Cosmochim Acta 35:801–824
- Hong YT et al (2005) Inverse phase oscillations between the East Asian and Indian Ocean summer monsoons during the last 12000 years and paleo-El Niño. Earth Planet Sci Lett 231:337–346
- Hu CY, Henderson GM, Huang JH, Xie SC, Sun Y, Johnson KR (2008) Quatification of Holocene Asian monsoon rainfall from spatially separated cace records. Earth Planet Sci Lett 266(3–4):221–232
- Huang RH, Li WJ (1987) Influence of the heat source anomaly over the tropical western Pacific on the subtropical high over East Asia. In: Proceedings of international conference on the general circulation of East Asia, Chengdu, pp 40–51
- Huang RH, Sun FY (1992) Impact of the tropical western Pacific on the East Asian summer monsoon. J Meteorol Soc Jpn 70:243–256
- Huang RH, Huang G, Wei ZG (2004) Climate variations of the summer monsoon over China. In: Chang C (ed) The East Asian monsoon. World Scientific, Singapore, pp 213–268
- Johnson KR (2011) Palaeoclimate: long-distance relationship. Nat Geosci 4:426–427
- Johnson KR, Ingram BL, Sharp DW, Zhang PZ (2006) East Asian summer monsoon variability during marine isotope stage 5 based on speleothem δ^{18} O records from Wanxiang Cave, central China. Palaeogeogr Palaeoclimatol Palaeoecol 236:5–19
- Kanner LC, Burns SJ, Cheng H, Edwards RL (2012) High-latitude forcing of the South American summer monsoon during the last glacial. Science 335:570–573



- Kathayat G et al (2016) Indian monsoon variability on millennialorbital timescales. Sci Rep 6:24374. https://doi.org/10.1038/ srep24374
- Kleppin H, Jochum M, Otto-Bliesner B, Shields CA, Yeager S (2015) Stochastic atmospheric forcing as a cause of Greenland climate transitions. J Clim 28:7741–7763
- Li Y, Wang NA, Zhou XH, Zhang CQ, Wang Y (2014) Synchronous or asynchronous Holocene Indian and East Asian summer monsoon evolution: a synthesis on Holocene Asian summer monsoon simulations, records and modern monsoon indices. Global Planet Chang 116:30–40
- Li XL et al (2017a) The East Asian summer monsoon variability over the last 145 years inferred from the Shihua Cave record, North China. Sci Rep 7:7078. https://doi.org/10.1038/s41598-017-07251-3
- Li YX, Rao ZG, Cao JT, Jiang H, Gao YL (2017b) Highly negative oxygen isotopes in precipitation in southwest China and their significance in paleoclimatic studies. Quat Int 440:64–71
- Liu XD, Fang JG, Yang XC, Li XZ (2003) Climatology of dekadly precipitation around the Qinling mountains and characteristics of its atmospheric circulation. Arid Meteorol 21:8–13 (In Chinese with English abstract)
- Liu ZY et al (2014) Chinese cave records and the East Asia summer monsoon. Quat Sci Rev 83:115–128
- Liu JB, Chen JH, Zhang XJ, Li Y, Rao ZG, Chen FH (2015) Holocene East Asian summer monsoon records in northern China and their inconsistency with Chinese stalagmite δ^{18} O records. Earth Sci Rev 148:194–208
- Ma ZB et al (2012) The timing and structure of the Younger Dryas event in northern China. Quat Sci Rev 41:83–93
- Ma L, Cai YJ, Qin SJ (2015) A high resolution paleoclimate record of the last 2300 years in stalagmite QX-3 from the Qixing Cave, Guizhou Province. J Earth Environ 6:135–144 (In Chinese with English abstract)
- Maher BA (2008) Holocene variability of the East Asian summer monsoon from Chinese cave records: a re-assessment. Holocene 18:861–866
- Maher BA (2016) Palaeoclimatic records of the loess/palaeosol sequences of the Chinese Loess Plateau. Quat Sci Rev 154:23-84
- Maher BA, Hu MY (2006) A high-resolution record of Holocene rainfall variations from the western Chinese Loess Plateau: antiphase behaviour of the African/Indian and East Asian summer monsoons. Holocene 16(3):309–319
- Maher BA, Thompson R (2012) Oxygen isotopes from Chinese caves: records not of monsoon rainfall but of circulation regime. J Quat Sci 27:615-624
- Marchitto TM, Lehman SJ, Ortiz JD, Fluckiger J, Geen AV (2007) Marine radiocarbon evidence for the mechanism of deglacial atmospheric CO₂ rise. Science 316:1456–1459
- McGee D et al (2012) Lacustrine cave carbonates: novel archives of paleohydrologic change in the Bonneville Basin (Utah, USA). Earth Planet Sci Lett 351–352:182–194
- McManus JF, Francois R, Gherardi JM, Keigwin LD, Brown-Leger S (2004) Collapse and rapid resumption of Atlantic meridional circulation linked to deglacial climate changes. Nature 428:834–837
- Muschitiello F et al (2015) Fennoscandian freshwater control on Greenland hydroclimate shifts at the onset of the Younger Dryas. Nat Commun 6:8939. https://doi.org/10.1038/ncomms9939
- Novello VF et al (2017) A high-resolution history of the South American Monsoon from Last Glacial Maximum to the Holocene. Sci Rep 7:44267. https://doi.org/10.1038/srep44267
- O'Neil JR, Clayton RN, Mayeda TK (1969) Oxygen isotope fractionation in divalent metal carbonates. J Chem Phys 51:5547–5558

- Orland IJ, Edwards RL, Cheng H, Kozdon R, Cross M, Valley JW (2015) Direct measurements of deglacial monsoon strength in a Chinese stalagmite. Geology 43:555–558
- Parthasarathy B, Munot AA, Kothawale DR (1995) Monthly and seasonal rainfall series for all-India homogeneous regions and meteorological subdivisions: 1871–1994. Contributions from Indian Institute of Tropical Meteorology, Research Report RR-065, August 1995
- Pausata FSR, Battisti DS, Nisancioglu KH, Bitz CM (2011) Chinese stalagmite δ¹⁸O controlled by changes in the Indian monsoon during a simulated Heinrich event. Nat Geosci 4:474–480
- Peterson LC, Haug GH, Hughen KA, Röhl U (2000) Rapid changes in the hydrologic cycle of the tropical Atlantic during the Last Glacial. Science 290:1947–1951
- Rao ZG et al (2013) High-resolution summer precipitation variations in the western Chinese Loess Plateau during the last glacial. Sci Rep 3:2785. https://doi.org/10.1038/srep02785
- Romanov D, Kaufmann G, Dreybrodt W (2008) δ¹³C profiles along growth layers of stalagmites: comparing theoretical and experimental results. Geochim Cosmochim Acta 72:438–448
- Scholz D, Hoffmann DL (2011) StalAge—an algorithm designed for construction of speleothem age models. Quat Geochronol 6:369–382
- Sinha A et al (2005) Variability of southwest Indian summer monsoon precipitation during the Bølling–Allerød. Geology 33:813–816
- Sinha A, Berkelhammer M, Stott L, Mudelsee M, Cheng H, Biswas J (2011) The leading mode of Indian summer monsoon precipitation variability during the last millennium. Geophys Res Lett 38:L15703. https://doi.org/10.1029/2011GL047713
- Spötl C, Mangini A (2002) Stalagmite from the Austrian Alps reveals Dansgaard–Oeschger events during isotope stage 3: implications for the absolute chronology of Greenland ice cores. Earth Planet Sci Lett 203:507–518
- Stager JC, Ryves DB, Chase BM, Pausata FSR (2011) Catastrophic drought in the Afro-Asian monsoon region during Heinrich event 1. Science 331:1299–1302
- Stott L, Timmermann A, Thunell R (2007) Southern hemisphere and deep-sea warming led deglacial atmospheric CO₂ rise and tropical warming. Science 318:435–438
- Sun YB, Wang XL, Liu QS, Clemens SC (2010) Impacts of postdepositional processes on rapid monsoon signals recorded by the last glacial loess deposits of northern China. Earth Planet Sci Lett 289:171–179
- Sun YB, Clemens SC, Morrill C, Lin XP, Wang XL, An ZS (2011) Influence of Atlantic meridional overturning circulation on the East Asian winter monsoon. Nat Geosci 5:46–49
- Talma AS, Vogel JC (1992) Late Quaternary paleotemperatures derived from a speleothem from Cango Caves, Cape Province, South Africa. Quat Res 37:203–213
- Tan M (2009) Circulation effect: climatic significance of the short term variability of the oxygen isotopes in stalagmites from monsoonal China. Quat Sci 29(5):851–862 (In Chinese with English abstract)
- Tan M (2011) Tread-wind driven inverse coupling between stalagmite $\delta^{18}O$ from monsoon region of China and large scale temperature-circulation effect on decadal to precessional timescales. Quat Sci 31:1086–1097 (In Chinese with English abstract)
- Tan M (2014) Circulation effect: response of precipitation δ^{18} O to the ENSO cycle in monsoon regions of China. Clim Dyn 42:1067–1077
- Tan LC, Cai YJ, Cheng H, An ZS, Edwards RL (2009) Summer monsoon precipitation variations in central China over the past 750 years derived from a high-resolution absolute-dated stalagmite. Palaeogeogr Palaeoclimatol Palaeoecol 280:432–439
- Tan LC, Yi L, Cai YJ, Shen CC, Cheng H, An ZS (2013) Quantitative temperature reconstruction based on growth rate of



- annually-layered stalagmite: a case study from central China. Quat Sci Rev 72:137–145
- Tan LC, Shen CC, Cai YJ, Lo L, Cheng H, An ZS (2014a) Trace-element variations in an annually layered stalagmite as recorders of climatic changes and anthropogenic pollution in Central China. Ouat Res 81:181–188
- Tan LC et al (2014b) Cyclic precipitation variation on the western Loess Plateau of China during the past four centuries. Sci Rep 4:6381. https://doi.org/10.1038/srep06381
- Tan LC et al (2015) Climate significance of speleothem δ^{18} O from central China on decadal timescale. J Asian Earth Sci 106:150–155
- Tan LC et al (2017) Decreasing monsoon precipitation in southwest China during the last 240 years associated with the warming of tropical ocean. Clim Dyn 48:1769–1778
- Tan LC et al (2018) Centennial- to decadal-scale monsoon precipitation variations in the upper Hanjiang River region, China over the past 6650 years. Earth Planet Sci Lett 482:580–590
- Tao SY, Chen LX (1985) The East Asian summer monsoon, paper presented at Proceedings of International Conference on Monsoon in the Far East, Tokyo Nov. 5–8
- Tao SY, Chen LX (1987) A review of recent research on the East Asian summer monsoon in China. In: Chang CP, Krisnamurti TN (eds) Monsoon meteorology. Oxford University Press, Oxford, pp 60–92
- Wang HJ, Chen HP (2012) Climate control for southeastern China moisture and precipitation. Indian or East Asian monsoon? J Geophys Res 117:D12109. https://doi.org/10.1029/2012JD0177 34
- Wang B, Lin H (2002) Rainy season of the Asian-Pacific summer monsoon. J Clim 15:386–396
- Wang YJ et al (2001) A high-resolution absolute-dated late pleistocene monsoon record from Hulu Cave, China. Science 294:2345–2348
- Wang YJ et al (2005) The Holocene Asian monsoon: links to solar changes and North Atlantic climate. Science 308:854–857
- Wang XF et al (2007) Millennial-scale precipitation changes in southern Brazil over the past 90,000 years. Geophys Res Lett 34:L23701. https://doi.org/10.1029/2007GL031149
- Wang YJ et al (2008) Millennial-and orbitalscale changes in the East Asian monsoon over the past 224,000 years. Nature 451:1090–1093
- Webster PJ et al (1998) Monsoons: processes, predictability, and the prospects for prediction. J Geophys Res Ocean (1978–2012) 103:14451–14510
- Wolff EW, Chappellaz J, Blunier T, Rasmussen SO, Svensson A (2010) Millennial-scale variability during the last glacial: the ice core record. Quat Sci Rev 29:2828–2838
- Wong CI, Breecker DO (2015) Advancements in the use of speleothems as climate archives. Quat Sci Rev 127:1–18
- Xu H, Hong YT, Hong B (2012) Decreasing Asian summer monsoon intensity after 1860 AD in the global warming epoch. Clim Dyn 39:2079–2088

- Yancheva G et al (2007) Influence of the intertropical convergence zone on the East-Asian monsoon. Nature 445:74–77
- Yang B, Kang SY, Ljungqvist FC, He MH, Zhao Y, Qin C (2014a) Drought variability at the northern fringe of the Asian summer monsoon region over the past millennia. Clim Dyn 43:845–859
- Yang XL et al (2014b) Holocene stalagmite δ¹⁸O records in the East Asian monsoon region and their correlation with those in the Indian monsoon region. Holocene 24:1657–1664
- Yi L, Shi ZG, Tan LC, Deng CL (2018) Orbital-scale nonlinear response of East Asian summer monsoon to its potential driving forces in the late Ouaternary. Clim Dyn 50:2183–2197
- Yonge CJ, Ford DC, Gray J, Schwarcz HP (1985) Stable isotope studies of cave seepage water. Chem Geol Isot Geosci 58:97–105
- Yuan DX et al (2004) Timing, duration, and transitions of the last interglacial Asian monsoon. Science 304:575–578
- Zhang R, Delworth TL (2005) Simulated tropical response to a substantial weakening of the Atlantic thermohaline circulation. J Clim 18:1853–1860
- Zhang PZ et al (2008) A test of climate, sun, and culture relationships from a 1810-year Chinese Cave record. Science 322:940–942
- Zhang HB et al (2016) Antarctic link with East Asian summer monsoon variability during the Heinrich Stadial–Bølling interstadial transition. Earth Planet Sci Lett 453:243–251
- Zhang WC et al (2018) The 9.2 ka event in Asian summer monsoon area: the strongest millennial scale collapse of the monsoon during the Holocene. Clim Dyn 50:2767–2782
- Zhou WJ et al (2001) Terrestrial evidence for a spatial structure of tropical-polar interconnections during the younger Dryas episode. Earth Planet Sci Lett 191:231–239
- Zhou WJ, Xie SC, Meyers PA, Zheng YH (2005) Reconstruction of late glacial and Holocene climate evolution in southern China from geolipids and pollen in the Dingnan peat sequence. Org Geochem 36:1272–1284
- Zhou HY, Zhao JX, Feng YX, Gagan MK, Zhou GQ, Yan J (2008) Distinct climate change synchronous with Heinrich event one, recorded by stable oxygen and carbon isotopic compositions in stalagmites from China. Quat Res 69:306–315
- Zhou HY et al (2014) Heinrich event 4 and Dansgaard/Oeschger events 5–10 recorded by high-resolution speleothem oxygen isotope data from central China. Quat Res 82:394–404
- Zhou X et al (2016) Catastrophic drought in East Asian monsoon region during Heinrich event 1. Quat Sci Rev 141:1–8
- Zhu QG, He JH, Wang PX (1986) A study of circulation differences between East-Asian and Indian summer monsoons with their interaction. Adv Atmos Sci 3:466–477

Publisher's Note Springer Nature remains neutral with regard to jurisdictional claims in published maps and institutional affiliations.

